Evolution of Octupole Deformation in Radium Nuclei from Coulomb Excitation of Radioactive ^{222}Ra and ^{228}Ra Beams

P. A. Butler,[1,*] L. P. Gaffney,[1,2] P. Spagnoletti,[3] K. Abrahams,[4] M. Bowry,[3,5] J. Cederkäll,[6] G. de Angelis,[7] H. De Witte,[8] P. E. Garrett,[9] A. Goldkuhle,[10] C. Henrich,[11] A. Illana,[7] K. Johnston,[2] D. T. Joss,[1] J. M. Keatings,[3] N. A. Kelly,[3] M. Komorowska,[12] J. Konki,[2] T. Kröll,[11] M. Lozano,[2] B. S. Nara Singh,[3] D. O'Donnell,[3] J. Ojala,[13,14] R. D. Page,[1] L. G. Pedersen,[15] C. Raison,[16] P. Reiter,[10] J. A. Rodriguez,[2] D. Rosiak,[10] S. Rothe,[2] M. Scheck,[3] M. Seidlitz,[10] T. M. Shneidman,[17] B. Siebeck,[10] J. Sinclair,[3] J. F. Smith,[3] M. Stryjczyk,[8] P. Van Duppen,[8] S. Vinals,[18] V. Virtanen,[13,14] N. Warr,[10] K. Wrzosek-Lipska,[12] and M. Zielińska[19]

[1]*University of Liverpool, Liverpool L69 7ZE, United Kingdom*
[2]*ISOLDE, CERN, 1211 Geneva 23, Switzerland*
[3]*University of the West of Scotland, Paisley PA1 2BE, United Kingdom*
[4]*University of the Western Cape, Private Bag X17, Bellville 7535, South Africa*
[5]*TRIUMF, Vancouver V6T 2A3 BC, Canada*
[6]*Lund University, Box 118, Lund SE-221 00, Sweden*
[7]*INFN Laboratori Nazionali di Legnaro, Legnaro 35020 PD, Italy*
[8]*KU Leuven, Leuven B-3001, Belgium*
[9]*University of Guelph, Guelph N1G 2W1 Ontario, Canada*
[10]*University of Cologne, Cologne 50937, Germany*
[11]*Technische Universität Darmstadt, Darmstadt 64289, Germany*
[12]*Heavy Ion Laboratory, University of Warsaw, Warsaw PL-02-093, Poland*
[13]*University of Jyvaskyla, P.O. Box 35, Jyvaskyla FIN-40014, Finland*
[14]*Helsinki Institute of Physics, P.O. Box 64, Helsinki FIN-00014, Finland*
[15]*University of Oslo, P.O. Box 1048, Oslo N-0316, Norway*
[16]*University of York, York YO10 5DD, United Kingdom*
[17]*Joint Institute for Nuclear Research, RU-141980 Dubna, Russian Federation*
[18]*Consejo Superior De Investigaciones Científicas, Madrid S28040, Spain*
[19]*IRFU CEA, Université Paris-Saclay, Gif-sur-Yvette F-91191, France*

(Received 15 November 2019; published 31 January 2020; corrected 19 May 2020)

There is sparse direct experimental evidence that atomic nuclei can exhibit stable "pear" shapes arising from strong octupole correlations. In order to investigate the nature of octupole collectivity in radium isotopes, electric octupole ($E3$) matrix elements have been determined for transitions in ^{222,228}Ra nuclei using the method of sub-barrier, multistep Coulomb excitation. Beams of the radioactive radium isotopes were provided by the HIE-ISOLDE facility at CERN. The observed pattern of $E3$ matrix elements for different nuclear transitions is explained by describing ^{222}Ra as pear shaped with stable octupole deformation, while ^{228}Ra behaves like an octupole vibrator.

DOI: 10.1103/PhysRevLett.124.042503

There are many theoretical and experimental indications that atomic nuclei can exhibit reflection asymmetry in the intrinsic frame, and observation of low-lying quantum states in many nuclei with even Z, N having total angular momentum and parity of $I^{\pi} = 3^{-}$ is indicative of the presence of octupole correlations (see Ref. [1] and references therein). Typically, the electric octupole ($E3$) moment for the transition to the ground state is tens of single-particle units, suggesting that the octupole instability arises from a collective effect and leads to a pear-shaped distortion of the nuclear shape. What is less clear, however, is whether in some nuclei this distortion is stable, i.e., the nucleus assumes a permanent pear shape, or whether it is dynamic and the nucleus undergoes octupole vibrations. Evidence has been presented that ^{224}Ra and ^{226}Ra have static octupole deformation on account of an enhancement in the $E3$ moment in these nuclei [2,3]. Large $E3$ moments have also been recently measured for neutron-rich barium isotopes, suggesting that, within the experimental uncertainty, these nuclei could have octupole deformation [4,5].

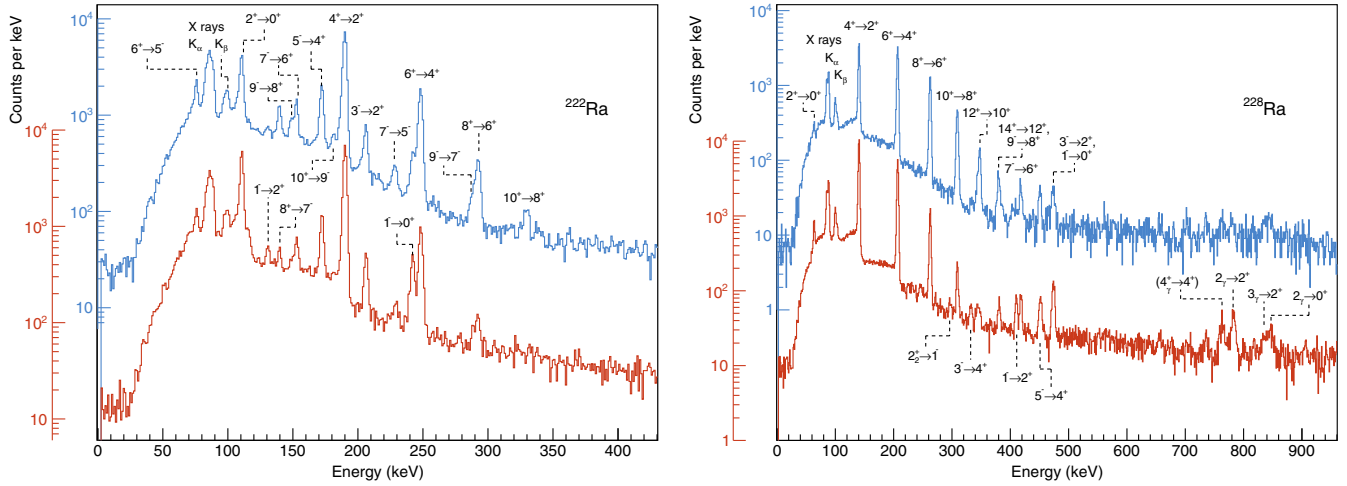

FIG. 1. Spectra of γ rays emitted following the Coulomb excitation of ^{222}Ra (left) and ^{228}Ra (right) using a ^{120}Sn target (blue, upper), and ^{60}Ni (red, lower). The γ rays were corrected for Doppler shift assuming that they are emitted from the scattered projectile. Random coincidences between Miniball and the silicon detector have been subtracted. The transitions that give rise to the observed full-energy peaks are labeled by the spin and parity of the initial and final states.

The only example of an octupole unstable nucleus other than ^{226}Ra where stable beams have been used to obtain a complete set of $E3$ matrix elements is ^{148}Nd [6].

In this Letter, results from a multistep, Coulomb-excitation experiment with radioactive ^{222,228}Ra beams are reported. By examining the pattern of $E3$ matrix elements between different transitions in these nuclei and comparing them to those in ^{224,226}Ra and ^{148}Nd, a distinction can be made between those isotopes having stable octupole deformation and those behaving like octupole vibrators. This observation is relevant for the search for permanent electric dipole moments in radium atoms [7–9], that would indicate sizable CP violation requiring a substantial revision of the standard model.

The radioactive isotopes ^{222}Ra ($Z = 88$, $N = 134$) and ^{228}Ra ($Z = 88$, $N = 140$) were produced by spallation in a thick uranium carbide primary target bombarded by $\approx 10^{13}$ protons/s at 1.4 GeV from the CERN PS Booster. The ions, extracted from a tungsten surface ion source were stripped to charge states of 51^+ and 53^+, respectively, for ^{222}Ra and ^{228}Ra and accelerated in HIE-ISOLDE to an energy of 4.31 MeV/nucleon. The radioactive beams, with intensities between 5×10^4 and 2×10^5 ions/s bombarded secondary targets of ^{60}Ni and ^{120}Sn of thickness 2.1 mg/cm^2. Gamma rays emitted following the excitation of the target and projectile nuclei were detected in Miniball [10], an array of 24 high-purity germanium detectors, each with sixfold segmentation and arranged in eight triple clusters. The scattered projectiles and target recoils were detected in a highly segmented silicon detector, distinguished by their differing dependence of energy with angle measured in the laboratory frame of reference. Representative spectra from the Coulomb-excited ^{222,228}Ra are shown in Fig. 1; in the spectra the γ-ray energies are corrected for Doppler shift assuming emission from the scattered projectile. The spectra were incremented when a target recoil was detected in coincidence with γ rays within a 450-ns time window; these data were corrected for random events. The fraction of the isobar ^{222}Fr in the beam was estimated to be about 20% by observing γ rays from the α-decay daughters at the beam dump. By lowering the temperature of the transfer line from the ion source a nearly pure beam of ^{222}Fr could be produced; apart from x rays, no discernable structure was observed arising from Coulomb excitation of the odd-odd nucleus in the particle-gated, Doppler-corrected spectrum. For the ^{228}Ra beam, the fraction of isobaric contamination was estimated to be $\approx 1\%$.

For both ^{222}Ra and ^{228}Ra the spectra reveal strong population of the ground-state band of positive-parity states, populated by multiple electric quadrupole ($E2$) Coulomb excitation, and substantial population of the octupole band of negative-parity states, populated by $E3$ excitation. The yields of the observed γ-ray transitions detected in Miniball were measured for four ranges of the recoil angle of the target nucleus for each target, between 21.5° and 55.5° for the ^{120}Sn target and between 17.8° and 55.5° for the ^{60}Ni target. The yield data were combined with existing γ-ray branching ratios to provide input to the Coulomb-excitation analysis code GOSIA [11–13]. The GOSIA code performs a least-squares fit to the $E\lambda$ ($\lambda = 1$, 2, 3) matrix elements (m.e.s), which either can be treated as free parameters, can be coupled to other matrix elements, or can be fixed. Energy-level schemes that are included in the

analysis are given in the Supplemental Material [14]. A total of 114 data for ^{222}Ra were fitted to 42 variables, while for ^{228}Ra 121 data were fitted to 41 variables. The starting values of each of the freely varied matrix elements were drawn randomly, within reasonable limits; the values obtained following the fitting procedure were found to be independent of the starting points. Examples of fits to the experimental data can be found in Ref. [14].

For both nuclei the $E1$ couplings between the ground-state and negative-parity bands and the $E2$ couplings for transitions within the ground state and within the negative-parity bands, with the exception of the $2^+ \rightarrow 0^+$ transition, were treated as free parameters. Under the experimental conditions described here, the probability of populating the 2^+ state is $> 90\%$ and it was not possible to determine the $\langle 0^+\|E2\|2^+\rangle$ and $\langle 2^+\|E2\|2^+\rangle$ m.e.s independently. The latter was therefore allowed to vary freely and the $\langle 0^+\|E2\|2^+\rangle$ matrix element was coupled to the $\langle 2^+\|E2\|4^+\rangle$ matrix element assuming the validity of the rotational model; this assumption is based on the behavior of nuclei where the lifetimes of the 2^+ and 4^+ states have been measured and for which the lowest transitions behave collectively [14]. For the $E3$ m.e.s the lowest couplings were treated as free parameters; m.e.s between higher-lying states, $\langle I^{\pm}\|E3\|I'^{\mp}\rangle$, were coupled to m.e.s between lower-lying states, $\langle (I-2)^{\pm}\|E3\|(I'-2)^{\mp}\rangle$, assuming the validity of the rotational model. $E4$ matrix elements were also included in the fitting procedure; these were calculated assuming the rotational model and a constant value of the hexadecapole moment, derived from the theoretical values of β_λ [22]. $E2$ (and magnetic dipole) couplings to high-lying $K^\pi = 0^+$ and $K^\pi = 2^+$ bands were also taken into account. The relative phase of $\mathcal{Q}_1$ and $\mathcal{Q}_3$ was investigated, as although the overall phase of the $E1$ and $E3$ matrix elements is arbitrary, the fit is sensitive to the relative phase of $E3$ matrix elements as well as the phase difference between the $E1$ and $E3$ matrix elements. The difference in chi-square for the fit favored $\mathcal{Q}_1$ and $\mathcal{Q}_3$ having the same sign for ^{222}Ra and the opposite sign for ^{228}Ra, and these phases were adopted in the final fits. These values are consistent with macroscopic-microscopic calculations [23] and constrained HFBCS calculations [24] that predict a decreasing value of $\mathcal{Q}_1$ with neutron number for radium isotopes, crossing zero for ^{224}Ra as experimentally verified [25].

Table I gives the values of $E2$ and $E3$ matrix elements for ^{222}Ra and ^{228}Ra obtained in this work. The $E1$ matrix

TABLE I. Values of $E2$ and $E3$ matrix elements measured in the present experiment. The intrinsic moments $\mathcal{Q}_\lambda$ are derived from each matrix element using $\langle I_i\|\mathcal{M}(E\lambda)\|I_f\rangle = \sqrt{(2I_i+1)}\sqrt{(2\lambda+1)/16\pi}(I_i 0\lambda 0|I_f 0)\mathcal{Q}_\lambda$. The uncertainties include the 1σ statistical error from the fit (χ^2+1 type) and the systematic contributions. The $E3$ m.e.s marked with an asterisk are coupled to higher-lying m.e.s. The $\langle 0^+\|E2\|2^+\rangle$ and $\langle 2^+\|E2\|4^+\rangle$ m.e.s are coupled. Values of $\mathcal{Q}_\lambda$ fitted assuming that the m.e.s are related by the rotational model are also given.

	^{222}Ra		^{228}Ra	
$\langle I\|E\lambda\|I'\rangle$	m.e. ($eb^{\lambda/2}$)	$\mathcal{Q}_\lambda$ (efm^λ)	m.e. ($eb^{\lambda/2}$)	$\mathcal{Q}_\lambda$ (efm^λ)
$\langle 2^+\|E2\|2^+\rangle$	-1.3 ± 0.5	330 ± 140	-0.3 ± 1.7	90 ± 400
$\langle 2^+\|E2\|4^+\rangle$	2.98 ± 0.15	590 ± 30	3.87 ± 0.19	770 ± 40
$\langle 4^+\|E2\|4^+\rangle$	-2.8 ± 0.5	580 ± 100		
$\langle 4^+\|E2\|6^+\rangle$	3.57 ± 0.18	559 ± 28	5.11 ± 0.26	800 ± 40
$\langle 6^+\|E2\|8^+\rangle$	4.15 ± 0.23	560 ± 30	5.89 ± 0.29	790 ± 40
$\langle 8^+\|E2\|10^+\rangle$	4.7 ± 0.5	560 ± 60	7.5 ± 0.4	890 ± 50
$\langle 10^+\|E2\|12^+\rangle$			$7.1^{+0.5}_{-0.3}$	770^{+60}_{-40}
$\langle 1^-\|E2\|3^-\rangle$	2.35 ± 0.22	560 ± 50	3.8 ± 0.5	890 ± 120
$\langle 3^-\|E2\|5^-\rangle$	3.1 ± 0.4	530 ± 70	$3.9^{+0.4}_{-0.8}$	670^{+70}_{-130}
$\langle 5^-\|E2\|7^-\rangle$	4.4 ± 0.4	630 ± 60	4.0 ± 0.9	580 ± 130
$\langle 7^-\|E2\|9^-\rangle$	6.0 ± 1.0	760 ± 120	5.9 ± 1.0	740 ± 130
$\mathcal{Q}_2$ (rotational model)		578 ± 18		798 ± 21
$\langle 0^+\|E3\|3^-\rangle$	1.13 ± 0.09	3030 ± 240	0.87 ± 0.15	2300 ± 400
$\langle 2^+\|E3\|1^-\rangle$	0.85 ± 0.24	2000 ± 600	$1.36 \pm 0.23^*$	3200 ± 600
$\langle 2^+\|E3\|3^-\rangle$	-0.9 ± 0.5	2100 ± 1200	$-0.06^{+0.23*}_{-0.16}$	150^{+360}_{-500}
$\langle 2^+\|E3\|5^-\rangle$	1.79 ± 0.20	3100 ± 400	$1.71 \pm 0.23^*$	3000 ± 400
$\langle 4^+\|E3\|1^-\rangle$	$-2.1 \pm 0.5^*$	4400 ± 1000	$0.4^{+0.7*}_{-1.1}$	-800^{+2300}_{-1400}
$\langle 4^+\|E3\|3^-\rangle$	$2.6^{+0.6*}_{-0.9}$	5500^{+1300}_{-1800}		
$\langle 4^+\|E3\|5^-\rangle$	$-1.7 \pm 1.0^*$	3200 ± 1800		
$\langle 4^+\|E3\|7^-\rangle$	$3.3^{+0.3*}_{-0.5}$	4600^{+500}_{-600}		
$\mathcal{Q}_3$ (rotational model)		3120 ± 190		2230 ± 290

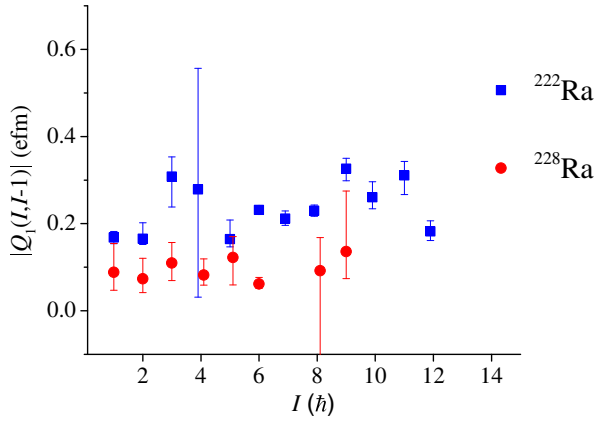

FIG. 2. Absolute values of the intrinsic dipole moments $\mathcal{Q}_1$ as a function of spin. The values are deduced from the measured matrix elements [14], and correspond to transitions between states with spin I and $I-1$.

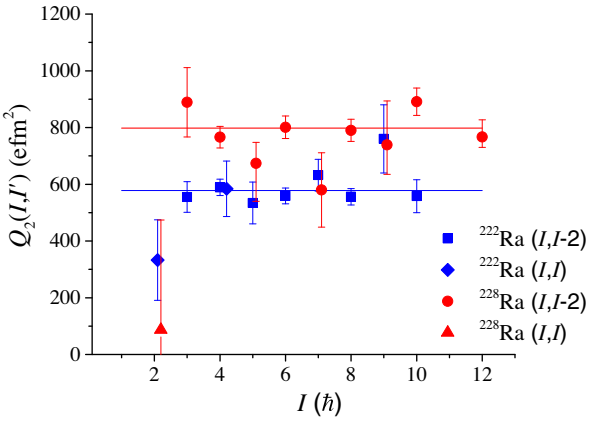

FIG. 3. Values of the intrinsic quadrupole moments $\mathcal{Q}_2$ plotted as a function of spin. The values are deduced from the measured matrix elements given in Table I. The values correspond to transitions between states with spin I and $I-2$; in some cases they are also derived from diagonal matrix elements. The solid horizontal lines correspond to the values of $\mathcal{Q}_2$ obtained assuming that the matrix elements are related by the rotational model.

elements are given in Ref. [14]. Those $E3$ m.e.s marked with an asterisk are coupled to m.e.s between higher-lying states and as such are not completely independently determined; however, the fit is mostly influenced by the value of the lowest matrix element. The diagonal $E2$ matrix elements are all coupled to the adjacent transition m.e.s except for those presented in Table I, which are independently determined. In the GOSIA fit the statistical errors for each fitted variable were calculated taking into account correlations between all variables. Independent sets of fitted values were also obtained by varying the constant hexadecapole moment used to calculate the $E4$ m.e.s between zero and double the notional value, varying the target thickness by $\pm 5\%$, the beam energy by $\pm 1\%$, the distance between the target and the particle detector by $\pm 7.5\%$, and the sign of the $E2$ couplings to the higher-lying collective bands.

The variations seen in the fitted values are included in the final uncertainties given in Table I. For ^{228}Ra the value of the intrinsic quadrupole moment, $\mathcal{Q}_2$, derived from the measured value of $\langle 2^+\|E2\|4^+\rangle$, 770 ± 40 efm^2, agrees with the values determined from the 2^+ lifetime, 775 ± 14 efm^2 and the 4^+ lifetime, 780 ± 6 efm^2, as reported in Ref. [16]. For ^{222}Ra, the value is 590 ± 30 efm^2, significantly smaller than the value derived from the measured lifetime of the 2^+ state, 673 ± 13 efm^2 [26]. It is noted that the value of $\mathcal{Q}_2$ for ^{222}Ra extrapolated from the 2^+ lifetime for ^{228}Ra on the basis of $B(E2;0^+ \rightarrow 2^+)$ systematics [27], is 593 ± 11 efm^2, in good agreement with the current measurement. Fitted values of $\mathcal{Q}_2$ and $\mathcal{Q}_3$ assuming that the $E\lambda$ matrix elements and $\mathcal{Q}_\lambda$ are related by the rotational model are also given in Table I. The values for $\lambda = 3$ indicate that the octupole collectivity in ^{228}Ra is significantly lower than for ^{222}Ra.

The values of $\mathcal{Q}_1$ and $\mathcal{Q}_2$ for all the measured matrix elements are shown in Figs. 2 and 3, respectively. The nearly constant values of $\mathcal{Q}_2$ as a function of spin for transitions in both positive- and negative-parity bands is consistent with stable quadrupole deformation. Smaller values of $\mathcal{Q}_2$, although with large uncertainty, were determined from the $\langle 2^+\|E2\|2^+\rangle$ matrix element for both nuclei. Such behavior was also observed in ^{226}Ra, interpreted as arising from deviations from axial symmetry [3]. The values of the intrinsic electric octupole moment $\mathcal{Q}_3$ for transitions in ^{222}Ra and ^{228}Ra are shown in Fig. 4. In the figure, the values of $\mathcal{Q}_3$ are shown separately for transitions $I^+ \rightarrow (I+1)^-$, $I^+ \rightarrow (I+3)^-$, $I^- \rightarrow (I+1)^+$, and $I^- \rightarrow (I+3)^+$, and are compared with values determined

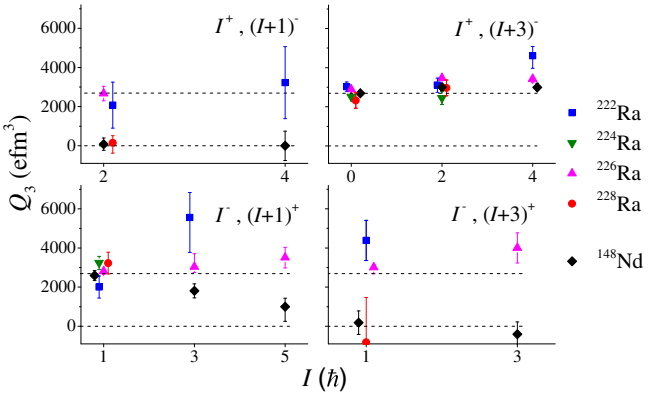

FIG. 4. Values of the intrinsic octupole moments $\mathcal{Q}_3$ plotted as a function of spin. The values are deduced from the measured matrix elements given in Table I. Here the values of $\mathcal{Q}_3$ are shown separately for transitions connecting $I^+ \rightarrow (I+1)^-$, $I^+ \rightarrow (I+3)^-$, $I^- \rightarrow (I+1)^+$, and $I^- \rightarrow (I+3)^+$. The upper dashed line is the average value of $\mathcal{Q}_3(0^+, 3^-)$ for the radium isotopes. To aid comparison, the values of $\mathcal{Q}_3$ for ^{148}Nd have been multiplied by 1.78.

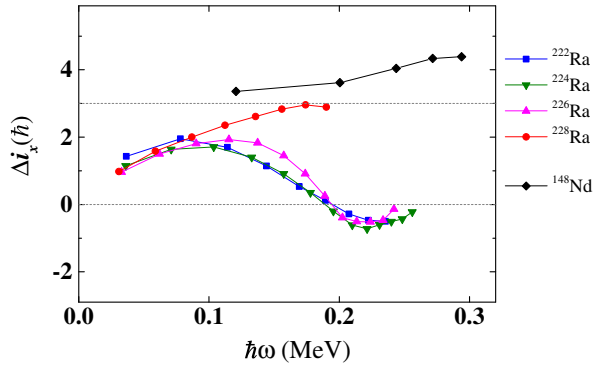

FIG. 5. The difference in aligned angular momentum, $\Delta i_x = i_x^- - i_x^+$, plotted as a function of rotational frequency ω. The upper dashed line corresponds to the vibrational limit, $\Delta i_x = 3\hbar$

for the same transitions in ^{224,226}Ra [2,3] and ^{148}Nd [6]. The values for ^{148}Nd are multiplied by a factor so that the value of $\mathcal{Q}_3$ deduced from $\langle 0^+ \| E3 \| 3^- \rangle$ is the same as the average value for the radium isotopes. It is observed that the values of $\mathcal{Q}_3$ for all transitions in ^{222,224,226}Ra are approximately constant, consistent with the picture of a rotating pear shape. In contrast, the values of $\mathcal{Q}_3$ corresponding to the $2^+ \to 3^-$ and $1^- \to 4^+$ transitions in ^{228}Ra are close to zero, as observed for ^{148}Nd. It is unlikely that this can be accounted for by K mixing [12] as the $K^\pi = 1^-$ band lies much higher in energy for these nuclei [28].

The contrast in the behavior of the $E3$ moments of ^{228}Ra (and ^{148}Nd) compared to the lighter radium isotopes is also present in the behavior of their energy levels, as shown in Fig. 5. Here Δi_x, the difference in aligned angular momentum between negative- and positive-parity states at the same rotational frequency ω, is plotted as a function of $\hbar\omega$ for the five nuclei. The behavior of Δi_x can reveal information regarding the nature of the octupole correlations [29,30]. For ^{148}Nd, the value of $\Delta i_x \sim 3\hbar$ for all values of rotational frequency, and for ^{228}Ra it approaches $3\hbar$ when $\hbar\omega \to 0.15$ MeV. This behavior is expected for octupole vibrators, where the octupole phonon aligns to the rotation axis. It is conjectured here that the observation of near-zero values of $\mathcal{Q}_3$ for some transitions in ^{228}Ra (and ^{148}Nd) is consistent with the octupole-vibrator description. The interpretation of the behavior of energy levels for ^{222,224,226}Ra in terms of rotating pear shapes is less obvious as it is dominated by pairing effects near the ground state; other interpretations of this behavior, e.g., the condensation of rotational-aligned octupole phonons [31], do not require the nucleus to have a permanent octupole distortion. On the other hand, highly collective $E2$ and $E3$ transition strengths are nearly independent of pairing and single particle effects and are a much better measure of the nuclear shape. The observed enhancement and rotorlike pattern of the electric octupole moments $\mathcal{Q}_3$ provide compelling evidence that ^{222}Ra together with ^{224,226}Ra have stable octupole deformation. This confirms theoretical predictions, e.g., Refs. [22,32,33], that the boundary of octupole deformation lies at $Z \approx 88$ and at $N \approx 138$; it has already been established that even-even radon ($Z = 86$) nuclei having similar neutron numbers behave like octupole vibrators [34]. It is concluded that the differing patterns of $E3$ matrix elements observed for ^{222,228}Ra are a consequence of the stability of the octupole shape for each nucleus. Any model of quadrupole-octupole coupling that describes this behavior should be capable of calculating values of $\mathcal{Q}_3$ for different $E3$ transitions including the critical $3^- \to 2^+$ transition, as has been performed for ^{224}Ra [35].

We are grateful to Doug Cline and the late Tomek Czosnyka who led the development of the Coulomb excitation analysis technique used in this work, and to Niels Bidault, Eleftherios Fadakis, Erwin Siesling, and Fredrick Wenander who assisted with the preparation of the radioactive beams. The support of the ISOLDE Collaboration and technical teams is acknowledged. This work was supported by the following Research Councils and Grants: Science and Technology Facilities Council (UK) Grants No. ST/P004598/1, No. ST/L005808/1, No. ST/R004056/1; Federal Ministry of Education and Research (Germany) Grants No. 05P18RDCIA, No. 05P15PKCIA, and No. 05P18PKCIA and the "Verbundprojekt 05P2018"; National Science Centre (Poland) Grant No. 2015/18/M/ST2/00523; European Union's Horizon 2020 Framework research and innovation programme 654002 (ENSAR2); Marie Skłodowska-Curie COFUND Grant (EU-CERN) 665779; Research Foundation Flanders and IAP Belgian Science Policy Office BriX network P7/12 (Belgium); GOA/2015/010 (BOF KU Leuven); RFBR (Russia) Grant No. 17-52-12015; and the Academy of Finland (Finland) Grant No. 307685.

*peter.butler@liverpool.ac.uk

[1] P. A. Butler and W. Nazarewicz, Rev. Mod. Phys. **68**, 349 (1996).
[2] L. P. Gaffney *et al.*, Nature (London) **497**, 199 (2013).
[3] H. J. Wollersheim *et al.*, Nucl. Phys. **A556**, 261 (1993).
[4] B. Bucher, S. Zhu, C. Y. Wu, R. V. F. Janssens, D. Cline *et al.*, Phys. Rev. Lett. **116**, 112503 (2016).
[5] B. Bucher, S. Zhu, C. Y. Wu, R. V. F. Janssens, R. N. Bernard *et al.*, Phys. Rev. Lett. **118**, 152504 (2017).
[6] R. W. Ibbotson *et al.*, Nucl. Phys. **A619**, 213 (1997).
[7] N. Auerbach, V. V. Flambaum, and V. Spevak, Phys. Rev. Lett. **76**, 4316 (1996).
[8] J. Dobaczewski, J. Engel, M. Kortelainen, and P. Becker, Phys. Rev. Lett. **121**, 232501 (2018).
[9] M. Bishof *et al.*, Phys. Rev. C **94**, 025501 (2016).
[10] N. Warr *et al.*, Eur. Phys. J. A **49**, 40 (2013).
[11] T. Czosnyka, D. Cline, and C. Y. Wu, Bull. Am. Phys. Soc. **28**, 745 (1983).

[12] D. Cline, Nucl. Phys. **A557**, 615 (1993).
[13] M. Zielińska, L. P. Gaffney, K. Wrzosek-Lipska, E. Clément, T. Grahn, N. Kesteloot, P. Napiorkowski, J. Pakarinen, P. Van Duppen, and N. Warr, Eur. Phys. J. A **52**, 99 (2016).
[14] See Supplemental Material at http://link.aps.org/supplemental/10.1103/PhysRevLett.124.042503 for details of the level-schemes, representative fitted yields, $E2$ systematics for the lowest transitions and values of the deduced $E1$ matrix elements, which includes Refs. [15–21].
[15] S Singh, A. K. Jain, and J. K. Tuli, Nucl. Data Sheets **112**, 2851 (2011).
[16] K. Abusaleem, Nucl. Data Sheets **116**, 163 (2014).
[17] T. Kibédi, T. W. Burrows, M. B. Trzhaskovskaya, P. M. Davidson, and C. W. Nestor, Jr., Nucl. Instrum. Methods Phys. Res., Sect. A **589**, 202 (2008).
[18] Evaluated Nuclear Structure Data File Search and Retrieval, https://www.nndc.bnl.gov/ensdf/.
[19] R. B. Cakirli, R. F. Casten, J. Jolie, and N. Warr, Phys. Rev. C **70**, 047302 (2004).
[20] G. Thiamova, D. J. Rowe, and J. L. Wood, Nucl. Phys. **A780**, 112 (2006).
[21] B. Sayği *et al.*, Phys. Rev. C **96**, 021301(R) (2017).
[22] W. Nazarewicz, P. Olanders, I. Ragnarsson, J. Dudek, G.A. Leander, P. Möller, and E. Ruchowsa, Nucl. Phys. **A429**, 269 (1984).
[23] P. A. Butler and W. Nazarewicz, Nucl. Phys. **A533**, 249 (1991).
[24] J. L. Egido and L. M. Robledo, Nucl. Phys. **A494**, 85 (1989).
[25] R. J. Poynter *et al.*, Phys. Lett. B **232**, 447 (1989).
[26] R. E. Bell, S. Bjørnholm, and J. C. Severiens, Mat. Fys. Medd. K. Dan. Vidensk. Selsk **32**, 12 (1960).
[27] B. Pritychenko, M. Birch, and B. Singh, Nucl. Phys. **A962**, 73 (2017).
[28] K. Neergård and P. Vogel, Nucl. Phys. **A145**, 33 (1970); **A149**, 217 (1970).
[29] J. F. C. Cocks, P. A. Butler, K. J. Cann, P. T. Greenlees, G. D. Jones *et al.*, Phys. Rev. Lett. **78**, 2920 (1997).
[30] P. A. Butler, J. Phys. G **43**, 073002 (2016).
[31] S. Frauendorf, Phys. Rev. C **77**, 021304(R) (2008).
[32] L. M. Robledo and P. A. Butler, Phys. Rev. C **88**, 051302(R) (2013).
[33] S. E. Agbemava, A. V. Afanasjev, and P. Ring, Phys. Rev. C **93**, 044304 (2016).
[34] P. A. Butler *et al.*, Nat. Commun. **10**, 2473 (2019).
[35] S. Y. Xia, H. Tao, Y. Lu, Z. P. Li, T. Nikšić, and D. Vretenar, Phys. Rev. C **96**, 054303 (2017).

Correction: A proof change request to replace two panels in Figure 1 was not implemented properly and has now been remedied.